Journal of Power Sources 202 (2012) 149–156

Contents lists available at SciVerse ScienceDirect

Journal of Power Sources

journal homepage: www.elsevier.com/locate/jpowsour

Compliant alkali silicate sealing glass for solid oxide fuel cell applications: The effect of protective YSZ coating on electrical stability in dual environment

Yeong-Shyung Chou*, E.C. Thomsen, J.-P. Choi, J.W. Stevenson

K2-44, Energy and Efficiency Division, Pacific Northwest National Laboratory, P.O. Box 999, Richland, WA 99354, United States

ARTICLE INFO

Article history:
Received 19 September 2011
Received in revised form 4 November 2011
Accepted 5 November 2011
Available online 23 November 2011

Keywords:
Sealing glass
Electrical stability
Resistivity
YSZ coating
SOFC

ABSTRACT

Recently, compliant sealing glass has been proposed as a potential candidate sealant for solid oxide fuel cell (SOFC) applications. In a previous paper, the thermal stability and chemical compatibility were reported for a compliant alkali-containing silicate glass sealed between anode supported YSZ bi-layer and YSZ-coated stainless steel interconnect. In this paper, we will report the electrical stability of the compliant glass under a DC load and dual environment at 700–800 °C. Apparent electrical resistivity was measured with a 4-ponit method for the glass sealed between two plain SS441 metal coupons or YSZ-coated aluminized substrates. The results showed instability with plain SS441 at 800 °C, but stable behavior of increasing resistivity with time was observed with the YSZ coated SS441. In addition, results of interfacial microstructure analysis with scanning electron microscopy will be correlated with the measured resistivity results. Overall, the YSZ coating demonstrated chemically stability with the alkali-containing compliant silicate sealing glass under electrical field and dual environments.

1. Introduction

Sealing for solid oxide fuel cells (SOFCs) remains a major challenge to advancing this emerging technology. To have SOFCs perform at high efficiency, hermetic seals or seals with low leakage are the first critical requirement. The requirement becomes more daunting when multiple tens (e.g., ~50–~100) of repeating cells are stacked together with alternating coated metallic interconnect plates to reach reasonable power levels in the kW range. SOFC sealing is complicated by the fact that there are different seal locations (perimeter, cell to window frame, and end plate), different mating materials (electrolyte and coated metallic interconnect), different temperatures and stress levels (transient, steady-state, and vibration), and dual oxidizing and reducing environments [1–10]. The sealant or sealants must meet the thermal, mechanical, physical, chemical, but also the electrical requirements. For glass seals, the challenges lie not only in the bulk properties, but also in establishing stable sealing interfaces without forming undesirable phases over long periods of time (up to 40,000 h).

The majority of SOFC glass seal research and development activities are focused on glass–ceramic approaches in which the initial glass devitrifies into a rigid or semi-rigid glass–ceramic mixture after the sealing processes [11–21]. Glass systems of alkaline earth-based aluminosilicate glasses have been extensively studied with regard to the physical properties [11,20], crystallization kinetics and the influence of nucleating agents [14], formulation and thermal properties [15,17–19], chemical compatibility with various SOFC components [12,13,16,21]. Other systems of composite glass [22–24] and phosphate glass [25] have also been investigated. Recently, a different approach based on compliant glass was proposed for SOFC application [5,26]. The compliant glass, as contrary to conventional glass–ceramics, is intended to remain vitreous without substantial crystallization, thereby retaining the softening or compliant behavior after sealing. As a result, this non-rigid behavior would relieve/reduce residual stresses, if any. In addition, should cracks form during cooling to room temperature they may heal upon re-heating. Crack healing has been observed in glasses at elevated temperatures [5,27,28]. However, the ability to maintain a vitreous state without crystallization at SOFC operation conditions over the long periods of time remains unknown. In our earlier work, an alkali-containing (K + Na ~17 mol%) compliant silicate sealing glass was studied in simple thermal cycling and isothermal ageing tests at elevated temperature sealed between YSZ electrolyte and aluminized SS441 metal substrate [26]. Results showed minimum reaction at YSZ and alumina interfaces, demonstrating the desired chemical compatibility. As mentioned earlier, the sealing glass must also satisfy electrical insulation requirements for SOFC application, not just the hermeticity. Given the fact that alkali ions are considered charge carriers for binary silicate glass, there is a need to investigate the electrical stability of the current alkali-containing silicate glass. In this paper, we will present electrical stability test results in terms of apparent

* Corresponding author. Tel.: +1 509 3752527; fax: +1 509 3752186.
E-mail address: yeong-shyung.chou@pnnl.gov (Y.-S. Chou).

0378-7753/$ – see front matter © 2011 Elsevier B.V. All rights reserved.
doi:10.1016/j.jpowsour.2011.11.017

resistivity versus temperature for the compliant glass sealed between two ferritic stainless steel (SS441) metal substrates under DC loading in dual environment. Both plain and YSZ-coated metal substrates were being tested. Of particular interest is the chemical compatibility of the glass with SOFC components such as YSZ electrolyte and metallic interconnect under an electrical field. Results of post-mortem microstructure and interfacial analysis will be discussed to assess the suitability of the compliant glass approach for SOFC applications.

2. Experimental

2.1. Chemical composition and thermal properties characterization

The glass under study is a commercial alkali silicate glass (SCN-1, SEM-COM, Toledo, OH). The silicate glass contains alkaline earths, mainly BaO (8.23 mol%) and CaO (3.34 mol%), alkalis of K_2O (10.0 mol%) and Na_2O (7.3 mol%), Al_2O_3 (2.8 mol%), and some impurities (less than 1%) of Fe, Mg and Ti. The glass has a relatively low transition temperature of 468 °C and softening point of 540 °C. The glass transition and softening points increased slightly to 486 °C and 600 °C, respectively, after three heating and cooling thermal cycles. The average coefficient of linear thermal expansion (CTE) was determined to be $\sim 11 \times 10^{-6}$/°K. The details of glass composition and thermal characterization are given in Ref [26].

2.2. Sample preparation and coupon sealing

A ferritic stainless steel, SS441 (ATI Allegheny Ludlum, Pittsburgh, PA), was selected for electrical stability tests. SS441 is a leading candidate for SOFC interconnect material due to its good oxidation resistance, matching CTE with ceramic parts, the formation of a conductive oxide scale, and reasonably low cost. The metal has a nominal composition of Cr (18% in wt%), Nb (0.5%), Mn (0.35%), Si (0.34%), Ni (0.3%), Ti (0.22%), and traces (<0.05%) of Al, P, S, N, and C [4]. Two metal coupons were sealed with each other with glass to form a test sample. The metal coupons were of square shape; one was 50 mm × 50 mm × 1 mm with a central hole of 6.4 mm diameter, while the other one was 25 mm × 25 mm × 1 mm. The metals were tested either in the as-received state or coated with YSZ and Al_2O_3. For SOFC application, the ferritic stainless steel SS441 requires a protective coating to prevent cathode poisoning due to Cr volatility, and seal degradation by forming chromates with very high CTEs if the sealing glass contains alkaline earths (e.g., Ba and Sr) [9,19,29]. In this study we have adopted a novel reactive air aluminizing coating process involving ultrasonic spraying of SS441 substrates with a mixture of Al powders in a binder solution, followed by drying and oxidizing at 1000 °C for 1 h in air [30]. After the aluminization process, the metal coupon was further coated with YSZ powders a few times using the ultrasonic sprayer (Model Prism-350, USI, Haverhill, MA). The sample was then heat treated at 1000 °C for 1 h in air. To prevent the low viscosity sealing glass from potential spreading, two square phlogopite mica rings (~225 μm thick) with different sizes were cut from commercial mica papers. Test specimens were prepared by applying the glass paste between the two mica square rings on the large metal coupon (Fig. 1A) followed by application of the small coupon. After drying at 70 °C, the specimens were slowly heated to 550 °C for 2 h to remove organic binders in air. They were then fired to 800 °C for 2 h for final sealing under a compressive load. After cooling to room temperature, the joined metal couples (Fig. 1B) were tested for leakage by applying a small amount iso-propanol in the central cavity to observe any penetration of the alcohol to the other side. All joined couples used in electrical stability tests showed no alcohol penetration, indicating a hermetic seal.

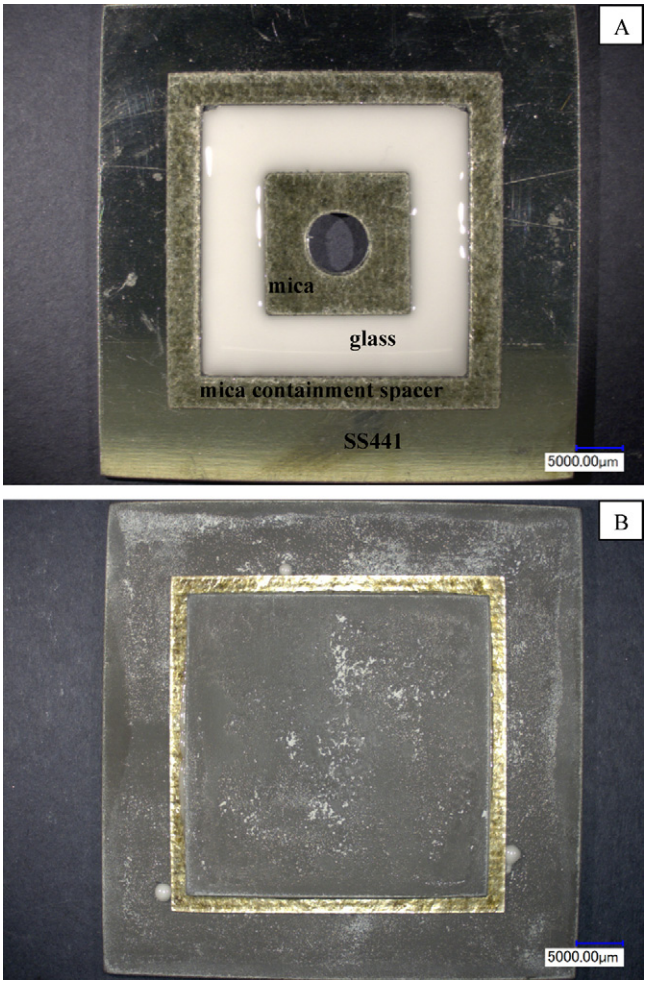

Fig. 1. Optical micrograph showing the sample preparation for coupon sealing. (A) Glass paste (white) applied between two mica square rings (dark green) on plain SS441 substrate with a central hole, and (B) test coupon after 800 °C for 2 h sealing. (For interpretation of the references to color in this figure legend, the reader is referred to the web version of the article.)

2.3. Electrical stability test in dual environment and characterization

A schematic drawing of the electrical stability test is shown in Fig. 2, detailing the perimeter seal, the gas chamber, and the electrical connections. A hybrid mica seal with Ag interlayers was used as the perimeter seal, which demonstrated long-term stability up to 28,366 h at 800 °C as well as stability over 1000 thermal cycles [31]. Four Pt-wires were spot-welded onto the sealed couples, two on the smaller central square and two on the larger square but on the opposite side. A DC load of 0.8 V was applied with a commercial power supply (Agilent E3632A, Santa Clara, CA) on the sample. A resistor was also connected in series to measure the current through the voltage drop with a multimeter (Aligent 34970A, Santa Clara, CA). Three temperatures were chosen for the electrical stability tests: 700, 750, and 800 °C. The samples were exposed to dual environment where a reducing gas (5% H_2 in N_2 with ~3% H_2O) was flowing inside the test fixture and the other side was exposed to ambient air. After the test, the samples were characterized with optical microscopy. Some of the samples were also epoxy mounted, sectioned, and polished for interfacial characterization using scanning electron microscopy (SEM) and energy dispersive spectroscopy (EDS) (JEOL SEM model 5900LV).

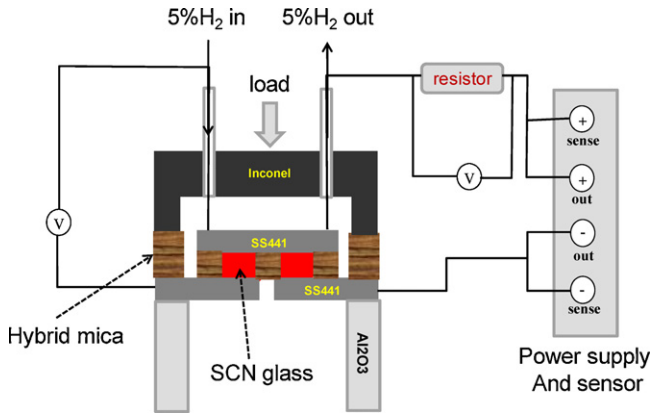

Fig. 2. Schematic drawing showing the electrical stability test set-up. Note the sample resistance was calculated based on voltage drop across a known resistor in series with the sample, and the tubing for incoming and outgoing reducing gas (5%H_2) is also used for leak testing with high purity helium at elevated temperatures.

3. Results and discussion

3.1. Electrical stability test of compliant glass with plain SS441 substrates

Fig. 3 shows the electrical stability results of the compliant sealing glass with as-received SS441 substrates in terms of apparent electrical resistivity versus time at various temperatures. In this work "apparent" resistivity was used since the measured resistance included not only the resistance of the compliant glass but also the resistance of the SS441 substrates and oxide scales, as well as potential interfacial phases formed between the glass and metal. Ferritic stainless steels are known to form a conductive oxide scale upon oxidation. The scale is composed of a primary continuous Cr_2O_3 layer and a discrete thin (Mn, Cr) mixed oxide [9]. As a result, the resistance contribution from the two SS441 substrates and two oxide scales can be neglected, and the measured resistivity was attributed to the compliant glass, since interfacial phases were not determined yet. From Fig. 3, it is evident that the compliant glass did not have the desired electrical stability at higher temperatures of 750 and 800 °C, while it showed steady behavior at 700 °C. For samples at 750 and 800 °C, the apparent resistivity increased initially till ~220 h, then started decreasing till ~250 h, and, after rapidly decreasing at around 350 h, remained fairly constant till ~500 h.

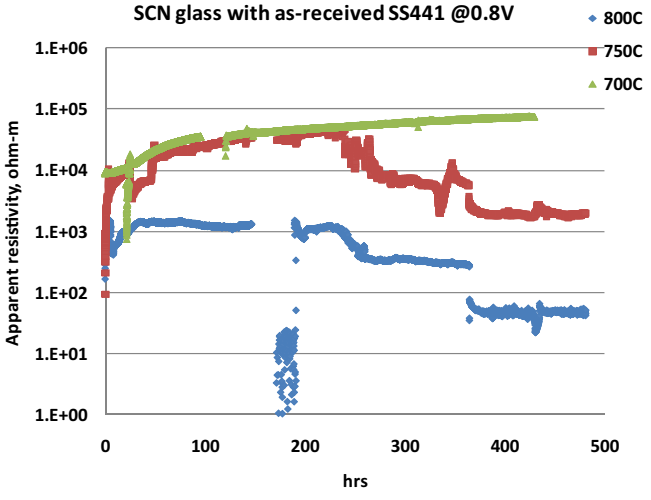

Fig. 3. Electrical stability test of SCN-1 glass with as-received SS441 substrate under a DC load of 0.8 V at elevated temperatures with flowing reducing gas (5%H_2 in N_2).

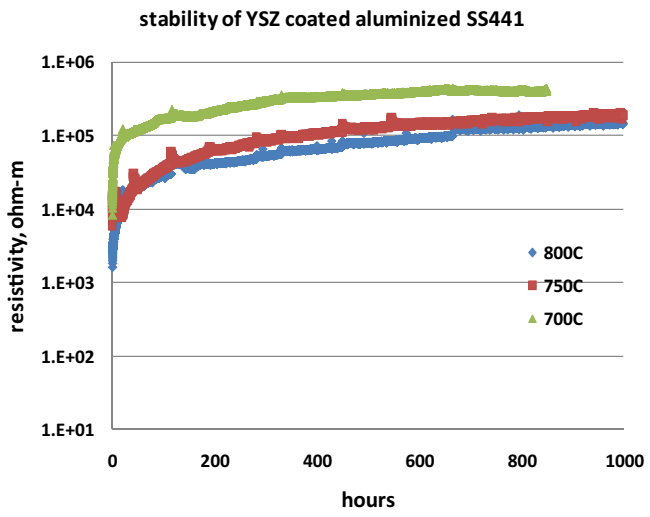

Fig. 4. Electrical stability test of SCN-1 glass with YSZ coated aluminized SS441 substrate under a DC load of 0.8 V at elevated temperatures with flowing reducing gas (5%H_2 in N_2).

Similar unstable resistivity behavior versus ageing time was also reported for Ba–Ca–Si glass with small additives of (Al, B-, Zn, V, and Pb) as well as the G18 glass [12,32]. The drastic drop in resistivity for the sample tested at 800 °C at ~200 h (from ~1000 Ω m to ~1 Ω m) is not clear. This is likely due to connection issues since the resistivity reversed to the original values after that short period of time. Nonetheless, the compliant glass did show the typical temperature dependence behavior as common silicate glasses or oxides in that the resistivity decreased as temperature increased.

It is interesting to note that the apparent resistivity of the compliant alkali-containing silicate glass was lower than the typical refractory-type sealing glass which crystallizes rapidly after initial sealing process. For example, the apparent resistivity of a refractory Sr–Ca–Y–B–Si sealing glass after ageing for 500 h was ~1.54×10^5 Ω m at 750 °C and ~3.21×10^4 Ω m at 800 °C [32], while the resistivity of the compliant glass after ageing for ~400 h was ~50Ω m (800 °C), 1.9×10^3 Ω m (750 °C), and 7.14×10^4 Ω m (700 °C). This is not surprising since the compliant glass does not crystallize substantially and remains fairly vitreous. In addition, the glass contains appreciable amount of alkalis (~17 mol%) which are considered charge carriers for typical binary alkali-silicate glasses. One can estimate the activation energy for electrical conduction of the compliant glass using the Arrhenius plot of ln(1/resistivity) versus 1/T(°K). The calculated activation energy was ~630 kJ mol^{-1} for data at ~400 h, and ~440 kJ mol^{-1} for data at ~300 h. The activation energy of electrical conduction for a typical refractory (non-crystallizing) alkaline-earth silicate sealing glass was found to be ~230 kJ mol^{-1} [32], ~110 kJ mol^{-1} for fused silica, ~140 kJ mol^{-1} for CaO–SiO_2, and ~310 kJ mol^{-1} for 98% polycrystalline magnesia [33,34]. The fact that the activation energy is not constant with time and very high values are obtained suggests microstructure evolution as well as compositional change within the current compliant glass. Indeed, the glass microstructure did crystallize and some foreign elements were identified, as discussed in the next sections.

3.2. Electrical stability test of compliant glass with YSZ and Al_2O_3 coated SS441 substrates

Fig. 4 shows the apparent resistivity of the compliant glass with the YSZ coated aluminized SS441 substrates at various temperatures. Clearly, the glass appears to be stable without the short-circuiting-like behavior observed in Fig. 3 for 800 °C data.

The apparent resistivity showed a gradual increase with time for all three temperatures tested, with more increase in the beginning ~100 h, similar to a refractory alkaline earth sealing glass [32]. The resistivity values at ~400 h were 6.46×10^4 Ω m (800 °C), 1.05×10^5 Ω m (750 °C), and 3.41×10^5 Ω m (700 °C), much higher than those for plain SS441 substrates (Fig. 3). As mentioned in the experimental section, the SS441 metal substrate was first aluminized; in this process the substrate was heat-treated at 1000 °C 1 h in air to form an Al_2O_3 layer, with varying thickness about 1 μm and less. The aluminized SS441 was then subjected to an ultrasonic spray of YSZ powders and fired to 1000 °C 1 h to promote densification and bonding to the alumina layer. At this low sintering temperature the YSZ coated layer is porous, and multiple coating runs were conducted which resulted in a thicker layer, about 10–15 μm. The electrical resistivity of dense YSZ at 800 °C is $\sim 2.5 \times 10^{-1}$ Ω m, so the resistance contribution from YSZ coating can be estimated to be ~0.02 Ω using an area of 5.16 cm^2, thickness of 15 μm, and 40% porosity. The contribution from the alumina layer cannot be accurately estimated, since the oxide layer also contains other elements (see chemical analysis in Section 3.4), so the resistivity could vary substantially from $\sim 10^3$ to $\sim 10^6$ Ω m. Clearly, the resistance from the alumina layer could not be ruled out as a contributor to the measured values. One can also estimate the activation energy for conduction using an Arrhenius plot of the resistivity at 300 h to be 184 kJ mol^{-1}, and 97 kJ mol^{-1} at 800 h. The change in activation energy with time is clearly directly related to the microstructure development as well as compositional change during crystallization. Nonetheless, compared to the active SOFC components, i.e., the cell, anode and cathode contacts, conductive coating and metallic interconnect, the resistivity of the compliant glass is much greater such that the loss of electrochemical performance by short-circuiting through the sealing glass would be very minute.

3.3. Interfacial microstructure characterization of compliant glass with plain SS441 substrates

The microstructure at the interface and within the glass matrix of the compliant glass with plain SS441 substrate after electrical testing at 800 °C and 700 °C for ~500 h is shown in Figs. 5 and 6, respectively. Fig. 5A shows the overall view of the glass between the two plain SS441 substrates, and Fig. 5B is a high magnification along the glass/metal interface of the 800 °C sample. Fig. 6A and B shows the overall view and glass/metal interface, respectively, for the 700 °C sample. It is evident that the compliant glass did crystallize to some extent, with more extensive precipitation at the lower temperature. At 800 °C there appears to be a single type of precipitates of gray color, while at 700 °C whitish needle-like particles are also present within the glass matrix. Six spots along the glass/metal interface and within the glass matrix were selected for EDS chemical analysis, and the results are listed in Tables 1 and 2 for 800 °C and 700 °C samples, corresponding to Figs. 5 and 6 B, respectively. For the 800 °C sample, the fracture occurred (likely during the ~500 h test when no gas bubbling was detected) between the thin (~1 μm) gray layer (#1 underneath the whitish band #2 in Fig. 5B). EDS showed a substantial amount of Si present, along with low content of Ti, Cr, and Fe from the metal substrate. No other elements from the compliant glass were detected. This may imply this thin layer is SiO_2 which has very low CTE (whether in the form of crystalline phase or amorphous) and contributed very high residual stresses leading to fracture. The whitish band (#2) was composed primarily of Cr and Si, along with small concentration of Fe, Mn, and Ti from the metal substrate. The color contrast within this ~5 μm band, which is not uniform but composed of white and gray phases, suggests corrosion behavior of compliant glass to the Cr oxide scale. The lack of distinct crystal morphology is also consistent with the

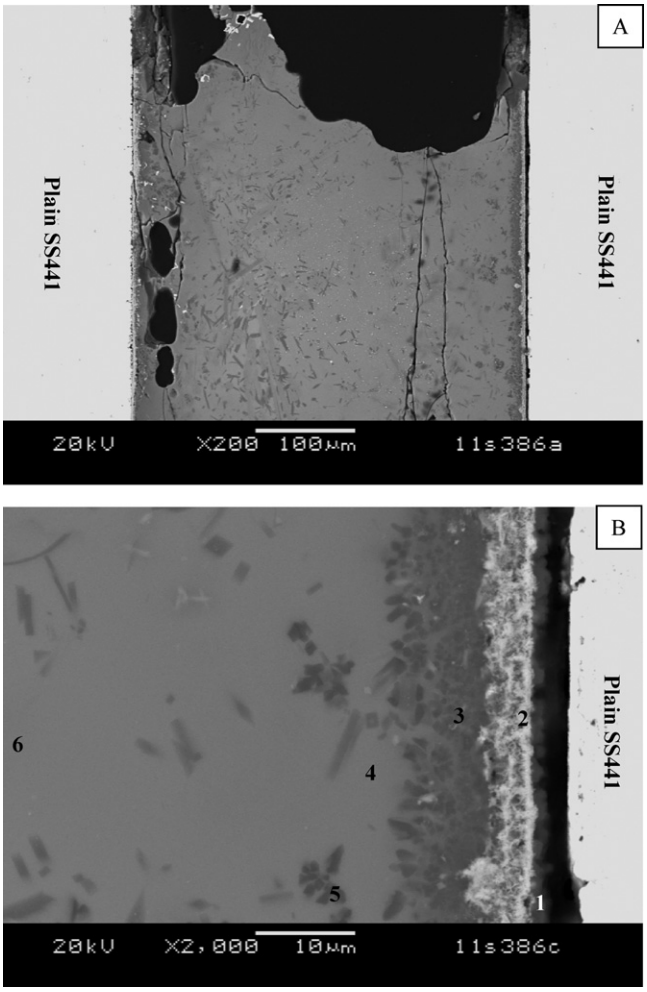

Fig. 5. Microstructure of the compliant glass with plain SS441 after electrical stability test at 800 °C for ~500 h. (A) Overall view, and (B) high magnification at interface.

fact that, according to phase diagrams, there is no stable compound between Cr_2O_3 and SiO_2. Away from the Si–Cr-containing whitish band, there are small gray precipitates (#3 and #5) composed primarily of the glass constituents and a small amount of some of the metal elements. Within the glassy (featureless) matrix (#4 and #6), a slightly higher amount of Fe was also detected (Table 1) than was detected in the gray precipitates. Similar diffusion of Fe was also identified in a previous study of G18 glass (a conventional glass–ceramic type sealing glass which crystallizes more rapidly over time) with a ferritic stainless steel (Crofer22APU). The apparent resistivity of G18 also showed decreasing behavior over a short period of time in an accelerated test at 830 °C, where the G18 glass has compliance similar to the SCN-1 glass tested in this study.

Compared to the 800 °C sample, the 700 °C sample showed much more crystallization with large needle-like gray precipitates and smaller white precipitates. The white precipitates were identified to be (Ba,Sr)-Si oxide, likely (Ba,Sr)SiO_3, a stable phase often observed in alkaline-earth silicate sealing glasses [13,17,32]. Near the glass/metal interface, the Cr-oxide scale was dense (unlike 800 °C sample in Fig. 5B) and consisted primarily of Cr with a much smaller content of Si as compared to the 800 °C sample (#1 in Fig. 6B and Table 2). The thin and dense Cr-oxide scale was able to withstand the corrosion of the compliant glass without forming the sponge-like microstructure and glass penetration though the oxide scale. This is likely due to less corrosive nature of the compliant glass at 700 °C. On the metal side (#2 and #3), near the interface, no trace elements of the glass were identified. The large gray

Table 1
Chemical composition (in at%) of selected spots in Fig. 5B for plain SS441 at 800 °C.

Spot #	O	Na	Mg	Al	Si	K	Ca	Ti	Cr	Mn	Fe	Ba
1	67.09				26.46			0.35	4.90		1.20	
2	65.41				13.52			0.84	19.43	0.51	0.29	
3	66.89	0.63	0.25	1.55	27.67	1.92	0.14	0.14	0.53		0.29	
4	64.84	2.24	0.61	1.54	24.90	3.32	0.86				0.70	1.00
5	65.83	0.95	0.31	1.28	28.26	2.04	0.37		0.10		0.38	0.48
6	64.44	2.43	0.69	1.25	24.84	3.17	1.23			0.15	0.50	1.31

Table 2
Chemical composition (in at%) of selected spots in Fig. 6B for plain SS441 at 700 °C.

Spot #	O	Na	Mg	Al	Si	K	Ca	Ti	Cr	Mn	Fe	Ni	Nb	Ba
1	62.07	0.96		0.31	4.60	0.43	0.25	0.52	28.50		1.98		0.38	
2	6.53				0.65				16.42		75.99	0.41		
3					0.53				17.67		81.81			
4	63.56	2.78	0.44	1.34	24.89	3.88	0.75			0.22	1.08			1.07
5	62.41	4.37	0.30	0.83	22.59	5.15	4.10	0.09			0.15			
6	63.99	2.84	0.66	1.41	24.92	3.70	0.72				0.56			1.20

precipitate (#5) has more alkalis than the glass matrix (#4 and #6). $KAlSi_3O_8$ has been identified as one of the two crystalline phases when the SCN-1 glass was isothermally aged for long period of time at elevated temperature [35]; however, the concentration from EDS (Table 2) does not correspond to this crystalline phase. It is also interesting to note that Fe was detected away from the glass/metal interface and at higher concentration in the glassy matrix than in the gray precipitates. This is similar to 800 °C sample; however, no Cr was detected within this region (about 30–40 μm away from glass/metal interface).

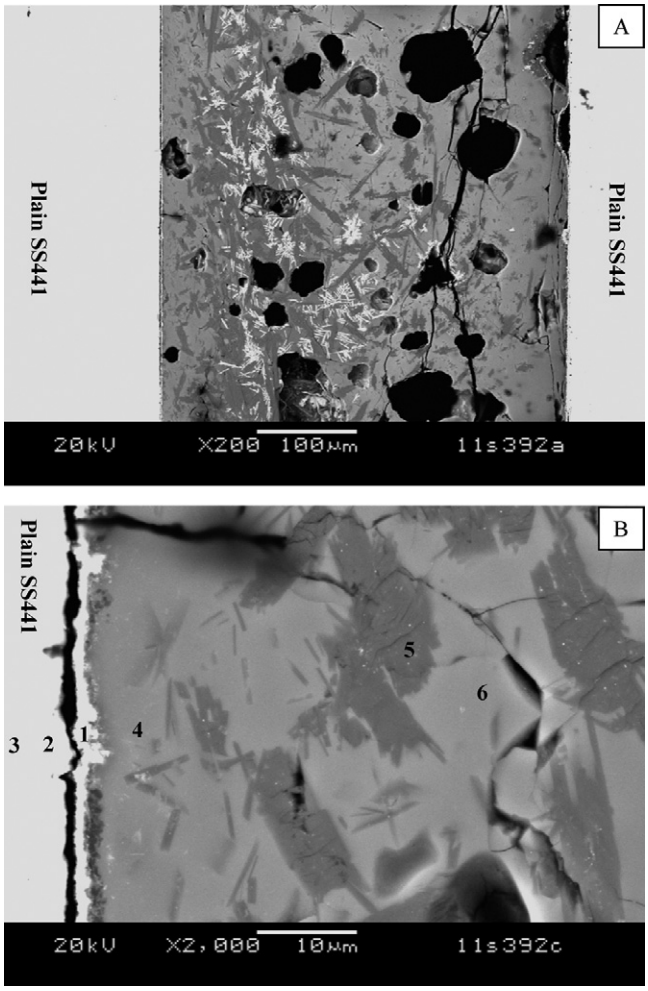

Fig. 6. Microstructure of the compliant glass with plain SS441 after electrical stability test at 700 °C for ~500 h. (A) Overall view, and (B) high magnification at interface.

3.4. Microstructure and interfacial characterization of compliant glass with YSZ and Al_2O_3 coated SS441 substrates

The interfacial microstructure of the compliant glass with YSZ-coated aluminized SS441 substrate after electrical testing at 800 °C for 1000 h and 700 °C for 850 h is shown in Figs. 7 and 8, respectively. Fig. 7A shows the overall view of the glass between the two YSZ coated SS441 substrates, and Fig. 7B is a high magnification along the glass/metal interface for the 800 °C sample. Fig. 8A and B shows the overall view and glass/metal interface, respectively, for the 700 °C. Clearly, the compliant glass showed similar crystallization with gray precipitates evenly distributed through the glass matrix. The volume fraction of the precipitates does not seem to increase distinctly with the ageing time when the sample was aged for ~1000 h (Fig. 7A) as compared to ~500 h for plain SS441 (Fig. 5A). However, the fracture occurred differently as compared to the plain SS441 substrate in that the fracture was primarily though the YSZ coating, rather than the compliant glass itself or the Cr-oxide scale. The cause for the fracture is likely two-fold: first, the YSZ coating was porous and hence weak, and second, the ultrasonic sprayer coating was conducted three times, which may have resulted in some defects between each run. Nonetheless, the compliant glass showed very good bonding to the YSZ coating. At high magnification of the glass/coating/metal interface region (Fig. 7B), five spots were selected for chemical analysis and the results are listed in Table 3. Spots #1 and #4 contain primarily Zr and Y, indicating the YSZ coating. The glass constituents are also detected within this white coating, indicating some penetration/diffusion of the compliant glass through the pores. The chemical compatibility of YSZ coating and the complaint glass appears satisfactory in that very low concentration of Zr was detected within the glass matrix nearby (spots #2 and #5), as well as the lack of features along the glass/YSZ coating interfaces. This is consistent with a previous study of SCN-1 glass with dense YSZ electrolyte in dual environment at 800 °C for 1000 h where no YSZ grains were found dissolved or corroded into the glass matrix [26]. For the dense YSZ electrolyte, it is not surprising that no reaction occurred along the glass/dense YSZ electrolyte interface since the YSZ electrolyte was typically sintered at 1400–1450 °C. As a result, the YSZ grains grew from initial submicron size to a few microns and formed a dense microstructure with less surface energy for sintering and reaction at low (800 °C)

Table 3
Chemical composition (in at%) of selected spots in Fig. 7B for YSZ-coated aluminized SS441 at 800 °C.

Spot #	O	Na	Mg	Al	Si	K	Ca	Cr	Mn	Fe	Y	Zr	Ba
1	71.73	0.63		0.92	4.26	0.94				0.29	3.22	18.02	
2	63.82	2.52		1.00	23.89	3.74	0.96		0.15	2.20		0.75	0.96
3	62.48	0.78		8.89	21.36	5.36		0.09		0.55		0.23	0.27
4	70.19			0.48	3.97	0.70					3.87	20.78	
5	64.07	1.99	0.55	1.45	26.60	3.38	0.97			0.16			0.84

temperature. Contrary to the dense YSZ electrolyte, the current coating using fine YSZ powders was only heat treated at 1000 °C for 1 h without substantial grain growth, and may still possess surface energy. The minimal reaction observed in Fig. 7B clearly demonstrated the desired chemical compatibility of YSZ with SCN-1 glass, though future optimization of coating thickness and microstructure would be needed. The compliant glass also showed penetration (likely through defects in the coating) under the YSZ coating, as shown by the chemical composition of spots #2 and #3, which contain an appreciable amount of the glass.

For the sample tested at 700 °C (Fig. 8), similar fracture through the YSZ porous coating was observed (Fig. 8A). There are two types of precipitates, gray and white needles, similar to the plain SS441 sample (Fig. 6A). The precipitates appear to be uniformly distributed, suggesting that the crystal nucleation and growth is volume controlled, rather than a surface dominated mechanism. EDS analysis of selected spots (#1–#4 Fig. 8B) is listed in Table 4. Within the porous YSZ coating, elements from the compliant glass were also detected (spot #1 Table 4). At the glass/YSZ interface, there is a thin gray layer and some whitish needles. The thin gray layer is composed primarily of the glass constituents with a very small amount of Zr (spot #2). Away from the interface (spots #3 and #4) the thick YSZ porous coating was able to block Cr diffusion into the glass matrix, as no Cr was detected.

3.5. Issues of alkalis in silicate sealing glass

It is known that for glasses containing significant concentrations of alkali oxides, particularly sodium, electrical current is carried almost entirely by alkali ions. The mobility of these ions is much larger than that of the network forming ions at all temperatures. This is true for simple binary and ternary glass systems. In this study, the SCN-1 compliant glass contains about 7 mol% Na_2O, 10 mol% K_2O, and six other elements in addition to Si. The complex

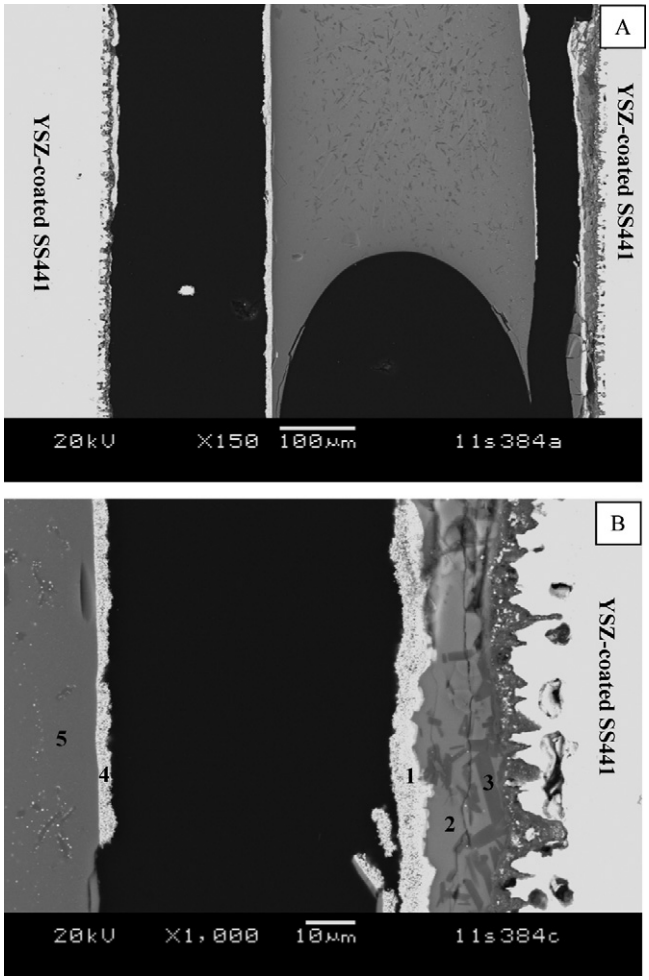

Fig. 7. Microstructure of the compliant glass with YSZ coated aluminized SS441 after electrical stability test at 800 °C for ~1000 h. (A) Overall view, and (B) high magnification at interface.

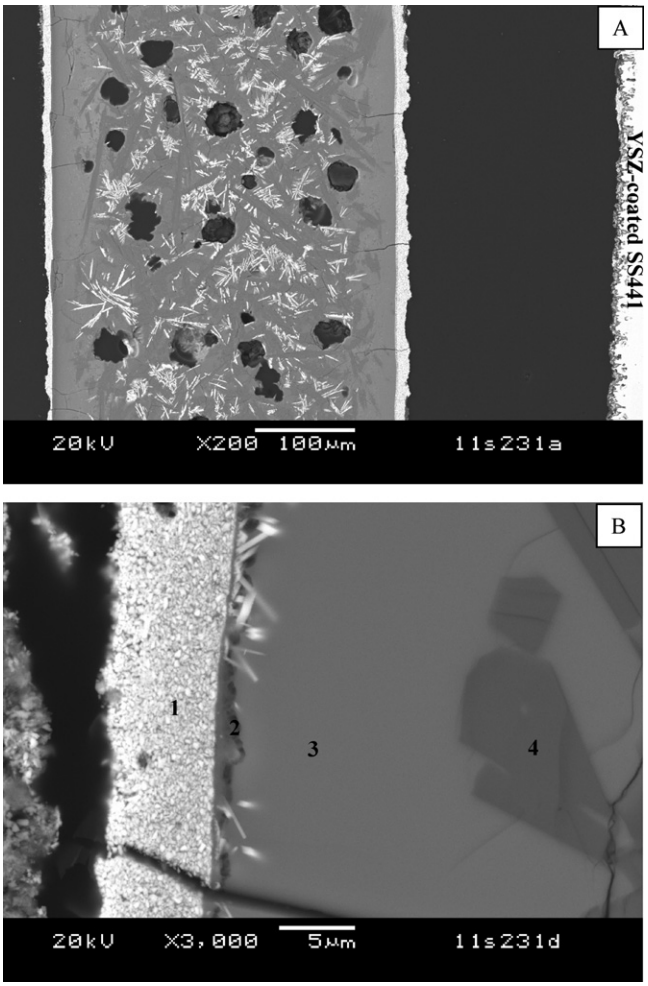

Fig. 8. Microstructure of the compliant glass with YSZ coated aluminized SS441 after electrical stability test at 700 °C for ~850 h. (A) Overall view, and (B) high magnification at interface.

Table 4
Chemical composition (in at%) of selected spots in Fig. 8B for YSZ-coated aluminized SS441 at 700 °C.

Spot #	O	Na	Mg	Al	Si	K	Ca	Fe	Zr	Ba	Ce
1	65.96	1.06		1.05	5.27	0.59	5.93	0.45	17.15	2.55	
2	60.64	8.12	0.34	0.94	19.59	3.07	4.16	0.14	1.75	0.94	0.33
3	60.62	7.04	0.85	1.60	21.54	5.51	1.24			1.59	
4	60.63	5.46	0.32		23.14	5.46	4.82			0.17	

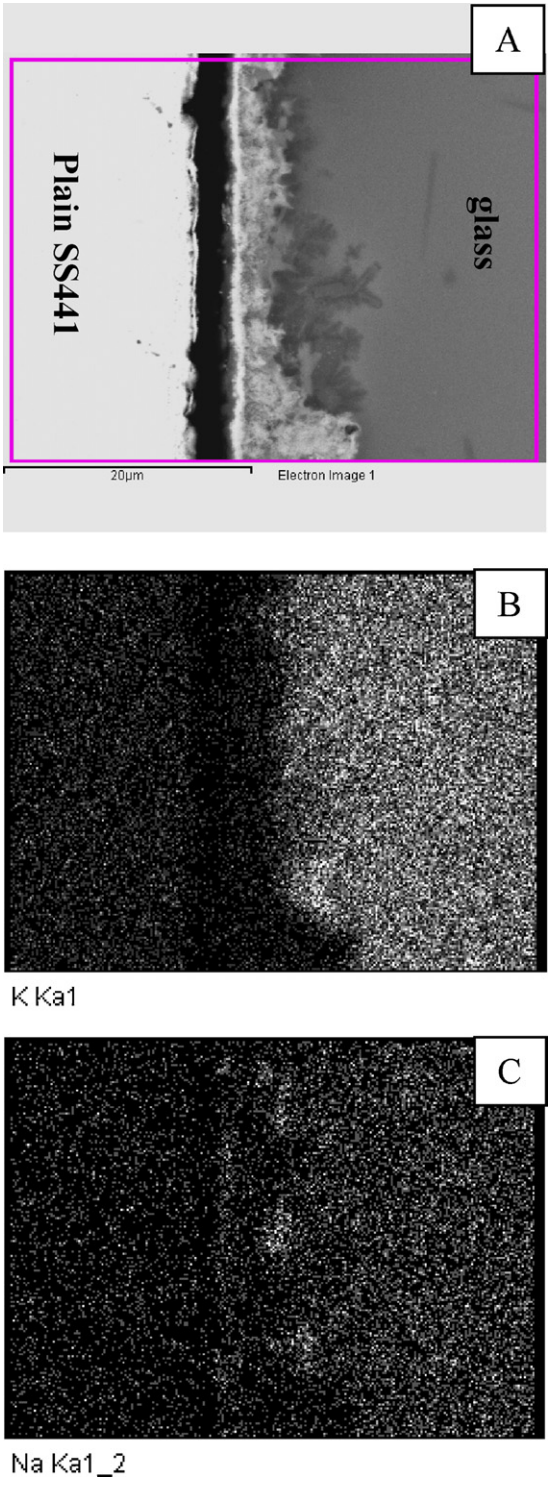

Fig. 9. Elemental mapping of alkalis near the glass/plain SS441 interface after 800 °C for 500 h electrical stability test. (A) SEM of the microstructure, (B) K mapping, and (C) Na mapping.

composition and the tendency of the constituents to crystallize and potentially interact with each other make the identification of charge carriers extremely difficult. Nonetheless, alkalis are often added in glass-making to lower the melting temperatures, and under an applied electrical field mobiles ions tend to move toward the electrode, so-called electrode polarization. It is possible alkalis may accumulate near the electrode (in this case one of the SS441 substrates), resulting in a different composition from the bulk of glass matrix. The localized higher concentration of alkalis could reduce the glass viscosity, and hence may lead to enhanced corrosion along the interfaces. Elemental mapping of Na and K along the glass/metal interfaces was therefore conducted on 800 °C tested samples where ions would have the highest mobility. The results shown in Fig. 9 indicate that no abnormal accumulation along the glass/metal interfaces was found for K and Na.

4. Summary and conclusions

A novel alkali-containing compliant silicate sealing glass for SOFC applications was evaluated in terms of electrical stability in dual environment. The glass was tested with both as-received and YSZ coated SS441 under DC loading. Results of apparent resistivity tests showed both stable behaviors with increasing resistance over time for the YSZ coated substrates. Unstable behavior was observed for the plain SS441 and was attributed to diffusion of elements from the SS441 substrate and microstructure evolution. Microstructure analysis showed fracture within the current YSZ coating; however, the coating was chemically compatible with the alkali-containing sealing glass. Elemental mapping also confirmed no segregation of alkalis along the glass/metal interfaces. Overall, the alkali-containing silicate glass was electrically stable against YSZ-coated SS441 substrates for SOFC applications.

Acknowledgements

The authors would like to thank S. Carlson and J. Coleman for SEM sample preparation and analysis. This paper was funded through the US Department of Energy's Solid-State Energy Conversion Alliance (SECA) Core Technology Program. Pacific Northwest National Laboratory is operated by Battelle Memorial Institute for the US Department of Energy under Contract no. DE-AC06-76RLO 1830.

References

[1] B.C.H. Steele, A. Heinzel, Nature 414 (6861) (2001) 345–352.
[2] N.Q. Minh, J. Am. Ceram. Soc. 76 (3) (1993) 563–588.
[3] M.C. Williams, J.P. Strakey, W.A. Surdoval, J. Power Sources 143 (1–2) (2005) 191–196.
[4] Y.-S. Chou, J.W. Stevenson, J.-P. Choi, Int. J. Appl. Ceram. Technol. 123 (2) (2010) 1–10.
[5] R.N. Singh, Int. J. Appl. Ceram. Technol. 4 (2) (2007) 134–144.
[6] P. Lessing, J. Mater. Sci. 42 (2007) 3465–3476.
[7] J.W. Fergus, J. Power Sources 147 (1) (2005) 46–57.
[8] C.-K. Lin, T.-T. Chen, Y.-P. Chyou, L.-K. Chiang, J. Power Sources 164 (1) (2007) 238–251.
[9] Z.-G. Yang, K.D. Meinhardt, J.W. Stevenson, J. Electrochem. Soc. 150 (8) (2003) A1095–A1101.
[10] Y.-S. Chou, J.W. Stevenson, J. Mater. Eng. Perform. 15 (4) (2006) 414–421.
[11] K.L. Ley, M. Krumpelt, R. Kumar, J.h. Meiser, I. Bloom, J. Mater. Res. 11 (6) (1996) 1489–1493.

[12] V.A.C. Haanappel, V. Shemet, I.C. Vinke, S.M. Gross, T.H. Koppitz, N.H. Menzler, M. Zahid, W.J. Quadakkers, J. Mater. Sci. 40 (7) (2005) 1583–1592.
[13] N. Lahl, D. Bahadur, K. Singh, L. Singheiser, K. Hilpert, J. Electrochem. Soc. 149 (5) (2002) A607–A614.
[14] N. Lahl, K. Singh, L. Singheiser, K. Hilpert, D. Bahadur, J. Mater. Sci. 35 (12) (2000) 3089–3096.
[15] S.-B. Sohn, S.-Y. Choi, G.-H. Kim, SongF H.-S., KimF G.-D., J. Non-Cryst. Solids 297 (2–3) (2002) 103–112.
[16] M.K. Mahapatra, K. Lu, J. Power Sources 196 (2) (2011) 700–708.
[17] K.D. Meinhardt, D.-S. Kim, Y.-S. Chou, K.S. Weil, J. Power Sources 182 (1) (2008) 188–196.
[18] S.-E. Lin, Y.-R.W.C. Cheng, J. Wei, J. Eur. Ceram. Soc. 31 (11) (2011) 1975–1985.
[19] Y.-S. Chou, J.W. Stevenson, P. Singh, J. Electrochem. Soc. 154 (7) (2007) B644–B651.
[20] P.K. Ojha, S.K. Rath, T.K. Chongdar, N.M. Gokhale, A.R. Kulkarni, J. Power Sources 196 (11) (2011) 4594–4598.
[21] M.K. Mahapartra, K. Lu, J. Power Sources 196 (2) (2011) 700–708.
[22] X. Qi, F.T. Akin, Y.S. Lin, J. Membr. Sci. 193 (2) (2001) 185–193.
[23] S. Taniguchi, M. Kadowaki, T. Yasuo, Y. Akiyama, Y. Miyake, K. Nishio, J. Power Sources 90 (1) (2000) 163–169.
[24] K.A. Nielsen, M. Solvang, S.B.L. Nielsen, A.R. Dinesen, D. Beeaff, P.H. Larsen, J. Eur. Ceram. Soc. 27 (2–3) (2007) 1817–1822.
[25] P.H. Larsen, P.F. James, J. Mater. Sci. 33 (10) (1998) 2499–2507.
[26] Y.-S. Chou, E.C. Thomsen, R.T. Williams, J.-P. Choi, N.I. Canfield, J.E. Bonnett, J.W. Stevenson, A. Shyam, E. Lara-Curzio, J. Power Sources 196 (5) (2011) 2709–2716.
[27] B.A. Wilson, E.D. Case, J. Mater. Sci. 32 (3) (1997) 3163–3175.
[28] W. Liu, X. Sun, M.A. Khaleel, J. Power Sources 185 (2) (2008) 1193–1200.
[29] Y.-S. Chou, J.W. Stevenson, P. Singh, J. Power Sources 184 (2) (2008) 1001–1008.
[30] J.-P. Choi, K. Scott Weil, Y.-S. Chou, J.W. Stevenson, Z.-G. Yang, Int. J. Hydrogen Energy 36 (7) (2011) 4549–4556.
[31] Y.-S. Chou, J.W. Stevenson, J. Power Sources 191 (2) (2009) 384–389.
[32] Y.-S. Chou, J.W. Stevenson, K.D. Meinhardt, J. Am. Ceram. Soc. 93 (3) (2010) 618–623.
[33] R.W. Wallace, E. Ruh, J. Am. Ceram. Soc. 50 (7) (1967) 358–364.
[34] M. Malki, P. Echegut, J. Non-Cryst. Solids 323 (1) (2003) 131–136.
[35] R. Trejo, E. Lara-Curzio, A. Shyam, M. Kirkham, V. Garcia-Negron, Y. Wang, Physical and mechanical properties of two barium alkali silicate glasses for SOFC sealing applications, unpublished work.